International Journal of Engineering

Journal Homepage: www.ije.ir

Probabilistic Damage Analysis of Isolated Steel Tub Girder Bridge Excited by Near and Far Fault Ground Motions

M. A. Baig*, M. I. Ansari, N. Islam, M. Umair

Jamia Millia Islamia, Department of Civil Engineering, New Delhi, India

PAPER INFO

Paper history:
Received 27 September 2022
Received in revised form 14 November 2022
Accepted 18 November 2022

Keywords:
Tub Girder Bridge
Friction Pendulum Isolator
Damage State
Probabilistic Demand Model
Fragility Curve

ABSTRACT

Friction Pendulum Bearing (FPB) has emerged as a popular solution for damage protection of bridges under seismic events. The study presents the probabilistic damage analysis for the isolated tub girder continuous bridge under the near and the far fault earthquakes using fragility analysis. The steel tub girder continuous bridge is considered with friction pendulum isolator as the seismic isolation mechanism. In order to represent the hysteretic behavior of friction pendulum isolators, a bilinear force-deformation model was used. Fragility curves are developed for various damage measures namely rotational ductility of pier and girder displacement with the peak ground acceleration (PGA) as an intensity measure (IM). Incremental dynamic analyses (IDA) were performed to develop the fragility curves and probabilistic damage model considering the four threshold damage states. The results suggest that in the case of low PGA level, the near fault earthquake leads to the high probability of exceedance in the case of isolated tub girder bridge. Damage model for piers and girder were developed to correlate component responses levels to overall bridge deterioration states. Finally, recommendations for the bridge developers in the stage of the early bridge seismic isolation design utilizing friction pendulum isolators are discussed.

doi: *10.5829/ije.2023.36.02b.09*

1. INTRODUCTION

In recent years, it is observed that the long-period displacement and velocity pulse motion of the near-fault earthquakes may severely influence the bridge seismic performance and design. Major earthquakes can inflict damage to them, which can have a large direct or indirect economic impact. The seismic isolation is considered to provide the layer of flexibility between the bent and the superstructure isolating the structure from the destructive force from the ground motion. Additional energy dissipation devices may also be utilized for increasing seismic response and reducing the damage to the bridges. The source of seismic excitation determines the dynamic response of the bridge structure and the designer must take this effect into consideration in order to produce a successful design [1].

The application of the friction pendulum dampers and the rubber bearings can prolong the superstructure vibration in response to earthquake motion leading to the increase the fundamental time period and lowering the likelihood that the structure will resonate when an earthquake occurs. During the swing of the friction pendulum back and forth, the friction between the wear plates may absorb some seismic energy [2].

Energy conservation was used in the numerical simulations for vibrations of continuous bridge using friction pendulum bearing (FPB) caused by the earthquakes. The multi-hazard source excitations (such as Taft and El Centro earthquake) with various dominating time- period and duration on an isolated bridge energy response, the impact of friction coefficient and the FPB isolation period was investigated [3].

Nonlinear dynamic history studies are performed to explore the sensitivity impacts of isolation duration, friction coefficient, limits on sliding deformation and the bridge reactions. The analysis shows that by employing proper friction coefficients, the drift and ductility may be

*Corresponding Author Institutional Email: aamirmirzagarri@gmail.com (M. A. Baig)

Please cite this article as: M. A. Baig, M. I. Ansari, N. Islam, M. Umair, Probabilistic Damage Analysis of Isolated Steel Tub Girder Bridge Excited by Near and Far Fault Ground Motions, ***International Journal of Engineering, Transactions B: Applications***, Vol. 36, No. 02, (2023), 289-298

reduced [4]. The ensemble of horizontal components of actual earthquake ground motions are studied in order to determine the seismic effect of multi-span continuous bridges decoupled by sliding isolators and elastomeric bearings. Different mathematical models of bridges isolated by various isolation techniques are provided with the mathematical framework for seismic response analysis [5].

Varied-sized seismic activity produces different levels of intensity in various seismic areas, and the severity of the damage to bridges caused by an earthquake directly relates to the intensity level. 1516 girder bridges and 612 arch bridges that were damaged to varying degrees by May 12, 2008 earthquake in Wenchuan County, China, were studied. The parameters of vulnerability assessment include sample number (SN), failure ratio (FR), and exceeding probability (EP) [6].

The empirical seismic damage probability matrix model together with a mean seismic damage index (MSDI) matrix model were computed in order to obtain a more realistic picture of the overall damage condition of various bridge segments. It was decided to use MSDI as the vulnerability parameter in a regional vulnerability matrix probability model [7].

The copula approach is used to create seismic fragility curves for isolated continuous girder bridges made of reinforced concrete, taking into account indices of earthquake damage such drift limit, isolated bearing, and main girder impact damage [8].

This study employs PSDM and the fragility analysis to investigate the probabilistic seismic damage analysis of a steel tub girder influenced by the ground vibrations from the near and the far faults. For parametric analysis, a benchmark bridge in New Delhi, India, that exhibits the essential features of a typical continuous girder bridge, was used. A nonlinear analytical model in three dimensions was created in the CSI Bridge software using bridge data to account for the inelastic behaviour of substructure. The IDA approach was utilized to compute damage for demand factors such as pier ductility and girder displacement, whereas seismic intensity parameters such as PGA were considered. The current study seeks to create an effective methodology for estimating the likelihood of collapse throughout the design and retrofit phases of bridges exposed to seismic risks.

2. GROUND MOTION CHARACTERISTIC AND SELECTION

Near-fault earthquakes (which are typically focused at a range of 10-20 km) include a substantial fraction of the fault energy appears as pulses. Far-field motions are defined as ground motions with an epicentral distance of greater than 10 miles [9]. When compared to higher frequencies of ground motions caused by the far-faults, near-fault ground motions have higher acceleration and more restricted frequencies. Seismic waves from such earthquakes often show lengthy pulse durations of large ranges in the beginning of earthquake records, particularly when they exhibit progressive direction effects. A significant amount of the fault energy is transferred to the site with a significant pulse that appears at the beginning of the seismic waves when the fault is propagating toward a site with a velocity that is similar to that of the shear wave [10].

Near-fault ground motions, according to Somerville are ones that frequently include pulses of long period velocity and persistent ground displacement. Most of the near-fault earthquake pulses have a maximum Fourier spectrum in a narrow range of periods, in contrast to far-field seismic events have a maximum Fourier spectrum throughout a wide range of periods [11].

The level of energy input to a structure is influenced by the seismic record rather than the structure's parameters [12]. To investigate the isolated bridge's behavior, 8 near-fault and 8 far-fault records of seismic events were selected from the Pacific Earthquake Engineering Research Center (PEER) database depicted in Table 1. Based on references, the following specific rules for choosing near-fault ground motion records were developed: (i) the nearest source-to-site distance to rupture in the chosen data were less than 10 km, which is typically thought to be within a near-fault region ; and (ii) the moment magnitude levels (Mw) were between 6 and 7.5 [13]. The epicentral distance of the far-field recordings taken into consideration was more than 20 km, and their magnitudes (Mw) ranged from 6 to 7.5. The response spectra for 5% damping for corresponding earthquakes is shown in Figure 1.

3. ISOLATION SYSTEM MODELING AND DESIGN

The Friction Pendulum (FPB) bearing has a spherical sliding interface and a spherical bearing (for the rotating

TABLE 1. Records of Near and Far Fault Earthquakes

Seismic Record	PGA	Near-fault Rjb	PGA	Far-fault Rjb	Mag.
	(g)	(Km)	(g)	(Km)	
Imperial	0.16	8.54	0.128	23.17	6.48
Irpinia	0.13	8.14	0.027	44.82	6.88
San Fernando	0.23	6.78	0.075	25.58	6.61
Loma Prieta	0.29	10.27	0.078	52.39	6.89
Northridge	0.41	0	0.047	53.71	6.69
Landers	0.73	2.19	0.115	69.21	7.28
Kobe Japan	0.35	3.31	0.068	69.04	6.86
Tabas Iran	0.62	1.46	0.105	24.07	7.35

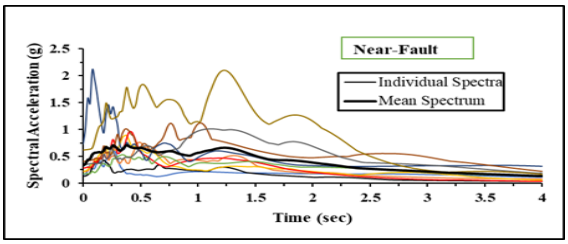

(a)

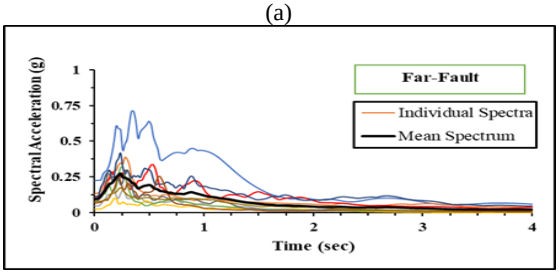

(b)

Figure 1. Response spectrums: (a) Near fault; (b) Far fault earthquakes

component). It functions very similarly to a spherical bearing having higher lateral stiffness as a result of the sliding interface curvature [14]. Such isolators may be made to have lengthy durations of vibration (5 or more seconds) and significant lateral displacement capabilities. The majority of friction pendulum bearings are made up of a concave spherical steel plate, an articulate slider, and a housing plate [5].

Two distinct processes work together to supply the bearing with resistance to horizontal loads that act to increase displacement. The first of these is the frictional resistance, F_f produced at the point where the articulated slider and concave surface meet. This force is determined by multiplying the weight component normal to the concave surface by the dynamic friction coefficient. A bilinear hysteresis model can roughly represent the (lateral) force- displacement behavior of an FPB, as shown in Figure 2. Figure 2 presents the representation of the equivalent linear stiffness (ke), which is determined by Equation (6). Equation (5) was used to calculate the period of vibration (Tp) that occurs after an FPB isolator is activated, where D_0 is the greatest value of the FPB horizontal displacement during the cyclic movement. Thus:

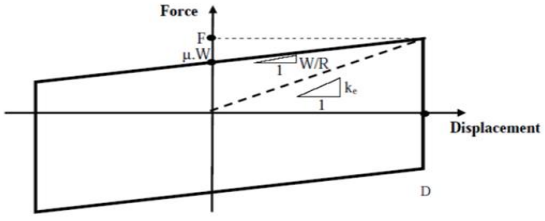

Figure 1. Idealized Bi-linear curve for Friction Pendulum Isolator

$$F_f = \mu W \cos\theta \quad (1)$$

The second mechanism of resistance is the bearing's restoring force, which is caused more by weight's tangential component and is provided by:

$$F_f = W \sin\theta \quad (2)$$

The following factors determine the bearing's horizontal resistance to displacement:

$$F = \mu W + \frac{W}{R} D \quad (3)$$

$$F = Q_d + K_d D \quad (4)$$

where μ = coefficient of friction; W = design load; R = Radius of concave sliding surface; Q_d = characteristic strength of isolator; D = design displacement and K_d = post yield stiffness of isolator.

The time period, while sliding is given by following expression:

$$T = 2\pi\sqrt{\frac{R}{g}} \quad (5)$$

By dividing the horizontal force, F, by the appropriate bearing displacement D, the effective isolator stiffness, ke, is determined as follows:

$$K_e = \frac{\mu W}{D} + \frac{W}{R} \quad (6)$$

The area of the hysteretic loop is given by Equation (7):

$$\text{Area} = 4\mu WD \quad (7)$$

The effective damping of the isolator is given by Equation (8):

$$\beta_e = \frac{2}{\pi}\left[\frac{\mu}{\mu + \frac{D}{R}}\right] \quad (8)$$

where β_e = effective damping of isolator.

4. METHODOLOGY FOR FRAGILITY FUNCTION

Bridges may sustain damage during an earthquake, especially if they were not constructed with proper seismic design and details. The uncertainty regarding a number of contributing variables and its capacity to sustain demands before incurring damage, it is appropriate to express the probability of experiencing various levels of damage using a probabilistic approach [15].

Fragility curves are classified into two types (i.e., empirical and analytical). Post-earthquake surveys are used to generate empirical fragility curves, which support to offer a broad understanding of correlation for the various structural damage limits and the ground motion indices [16]. This technique is impractical for creating fragility curves for bridges that have been modified

because damage state definitions are arbitrary and there is a scarcity of damage data. Analytical fragility curves that represent the seismic sensitivity of a structure have been developed using probabilistic seismic demand model (PSDM) that employ a Bayesian method and nonlinear time-history studies [17]. If the seismic demand and capacity were characterized by a log-normal distribution, the likelihood of attaining a certain damage state will also be distributed log-normally, as calculated by a cumulative log-normal probability density function as follows:

$$P\left[\frac{LS}{IM}\right] = \Phi\left[\frac{ln(IM) - ln\,(IM_n)}{\beta_{total}}\right] \quad (9)$$

where IMn = intensity measure median; ln (IM) logarithmic median of selected damage state; and Φ = standard cumulative normal distribution.

$$\beta_{total} = \sqrt{{\beta_C}^2 + {\beta_D}^2} \quad (10)$$

where β_C indicates the uncertainty of structural capacity and β_D indicates the uncertainty in ground motion.

In this study, the uncertainties in modelling, material characteristics, damping and concrete strength variations were not taken into account. The uncertainty due to earthquake ground vibrations was anticipated to be significantly larger than the uncertainties in structural capacity.

HAZUS specifies a value of βc of 0.3 for the isolated structure [18]. Based on these findings, a value of βc equal to 0.3 was used to create the fragility curves in this investigation.

A probabilistic seismic analysis was performed using a nonlinear time-history response analysis of the chosen bridge for the 16 ground motions. The PGA of the seismic records was scaled from 0.1g to 1.2g at intervals of 0.1g in this study to perform the IDA, which was utilized to construct the fragility curves. To identify the nonlinear behavior produced by the ground motions and to determine the variables of the conditional probability distribution of the demand measure, data from a total of 192 analyses were collated (i.e., pier ductility and the girder displacement). When predicated on the intensity measure, the demand measure data are considered to follow a lognormal distribution [19]. While the conditional demand dispersion is constant, the conditional mean of the given demand and (PGA) was linear in log-log space [20]. As a result, the resultant probabilistic seismic demand model (PSDM) was expressed by Equation (11):

$$\text{Demand Measure (DM)} = a\,(IM)^{b} \quad (11)$$

where DM = demand measure; IM = Intensity measure.

$$\ln DM = a + b \ln (PGA) \quad (12)$$

where a and b are regression coefficients on PGA and demand measure.

The suggested technique enables engineers to choose wisely by taking into account the likelihood of each restoration scenario reducing collapse[21].

5. DAMAGE METRICS AND THRESHOLD LIMITS

A limit state is the range beyond which the structure can no longer sustain the necessary level of performance. The most crucial damages for continuous girder seismically isolated bridges are the bridge piers and displacement of girder, which are frequently compelled to enter an inelastic range of deformation during earthquakes [22]. The seismic vulnerability evaluation of engineering structures often adopts the four HAZUS damage states of mild, modest, severe, and collapse damages [18]. The explanations behind the various damage states and the accompanying damage criteria that may be found in the literature are compiled in TABLE 2. Mild state depicts the structure yield point, past which plastic deformations occur to the structure, severe denotes the degree of damage to a bridge beyond which it would not be economically possible to rebuild it.

Collapse is the maximum load that a structure can bear before losing stability and perhaps collapsing completely or partially [23].

When considering earthquake-related bridge damage, excessive plastic rotation of the plastic hinges formed at the bridge pier is most frequently used. Inelastic rotation has been found to gradually reduce the stiffness and rigidity of the pier when they are subjected to seismic loads. It is thought that a reliable indicator of the damage is the ductility that results from inelastic rotation in the plastic hinge generated at the fixity points of piers [24]. The column ductility requirement is, by definition, stated as follows:

$$\varphi = \frac{\theta}{\theta_y} \quad (13)$$

where θy represents the equivalent rotation at the yield point and θ represents the rotation of pier in its plastic hinge.

The equivalent rotation at the yield point can be calculated as:

$$\theta_y = L_P * \varphi_y \quad (14)$$

$$Lp = 0.08L + 0.022\,fy * d \geq 0.044fy \quad (15)$$

where L_P depicts the length of plastic hinge, L depicts distance from inflection point to plastic hinge, d depicts steel bar diameter.

Using moment-curvature analysis, the plastic hinge length (Lp) was determined to be 0.765 m and ϕy to be 0.00025.

A bridge collapse will occur when the girder reaches its maximum seat length, which is determined by the

superstructure movement from the abutment. Due to the deck's longitudinal motion, girders may fall loose from the bearing pads, resulting in structural failure. From AASHTO-LRFD, the minimum seat width will be determined as follows [25]. The damage thresholds for mild, modest, severe, and collapse were considered with respect to the minimum seat width [26].

$$N = 1.5 \times \{8 + 0.002L + 0.008H\} \{1 + 0.000125 S^2\} \quad (16)$$

where N depicts minimum length of support length, L depicts deck length, and H depicts height of pier.

The damage limit state, which includes (i) pier ductility, which displays the inelastic rotations of bridge pier, and (ii) girder displacement, which displays the dislocation of girder from bearing, are regarded to correctly assess the vulnerability of the tub girder bridge. Four commonly utilized damage levels are employed in the seismic risk assessment of a chosen bridge:

6. FINITE ELEMENT MODELLING OF BRIDGE

The multi-span continuous (MSC) steel tub girder bridge used for this investigation has a continuous composite deck supported by concrete column bents. The bridge, which has four spans measuring 32.6, 38.7, 41.2, and 28.2 meters, as shown in Figure 3. The bridge's superstructure is made up of a continuous composite girder deck that is 10 m wide and 0.3 m thick, and it is supported by two tub girders that are 5 m apart [27]. The twin column bents made of reinforced concrete support the girders with height of pier 6.6m. The pier has a diameter of 1.6m and a 1.6 m by 1.25 m cap beam make up the concrete column bent. Each column is strengthened with 25 dia. #32 vertical bars and 150 mm-spaced #10 spiral hoops. The abutments support the girders at the ends of the bridge. Figure 3 depicts the cross sections of the tub girder, pier and cap beam.

For the purpose of simulating the superstructure and substructure of the bridge, the lumped mass approach was used. In the structural modelling of a steel box girder bridge, elastic beam elements were used to represent the girder, while nonlinear elements were used to simulate the bearings and piers [18]. Rigid links were used to connect the girder and piers with bearings, while fiber-based nonlinear links were used to represents the piers plastic hinge [28] . The ends of the columns are where plastic hinges are most likely to develop, as shown in Figure 8, and they are modelled using the lumped plasticity model [29]. The steel model uses the Menegotto-Pinto model of steel to replicate the reinforcing bars for the piers [30]. The characteristic strengths of steel reinforcing yield stress (415 MPa), confined concrete (45 MPa), and unconfined concrete (40 MPa). The bridges are simulated in three dimensions while taking into account geometrical and material nonlinearities utilizing a finite element programmed CSI Bridge.

The bents were assumed to be fixed at the base due to the stiff site consideration, and the effect of soil interaction was not considered [25].

TABLE 2. Damage Limit Definition

Damage Metrics	Damage Limits			
	Mild	Modest	Severe	Collapse
	DL-1	DL-2	DL-3	DL-4
Pier Ductility	2.01	3.14	5.90	9.42
Girder displacement	25% N	50% N	75% N	100% N

6. 1. Model for Friction Pendulum Isolator

The element non-linear links of the Isolator property type, which exhibit bilinear hysteretic behavior, were used to model the friction pendulum in the CSI Bridge. For the two shear directions, this element exhibits coupled bilinear hysteretic behavior, whereas the other four degrees of freedom (axial deformation and three rotations) are linear [31]. For friction isolator connections, the force-deformation curve characteristics are manually entered into the CSI Bridge data sheet depicted in Table 3. The isolator characteristics used in the study of isolated bridges determine effective stiffness. The fundamental period of a taken for isolated bridge is 2 seconds, whereas the period of a non-isolated bridge is 0.37 seconds.

7. RESULTS AND DISCUSSION

The Probabilistic damage analysis of a four-span continuous steel tub bridge isolated by a friction

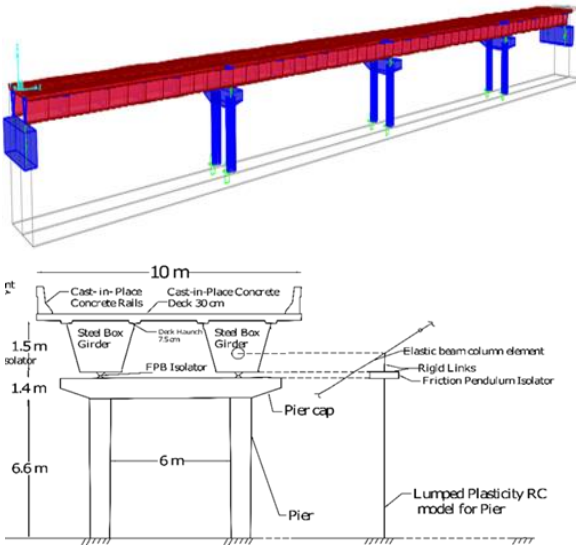

Figure 2. Finite element model of Tub girder bridge

TABLE 3. Friction pendulum Design parameters

Location	Radius	Eff. stiffness	Post slip stiffness	Coff. of Friction	Coff. of Friction	Eff. damping
	(m)	K_{eff} (KN/m)	K1 (KN/m)	μ fast	μ slow	β_{eff}
Abutment	1.2	848.2	669.16	0.04	0.02	0.134
Bent	1.2	2759.2	2176.6	0.04	0.02	0.134

pendulum isolator is assessed by developing bridge component fragility curves (pier and girder). The near and far fault earthquake records were scaled to a PGA of 0.1 g to 1.2 g, with 0.1g increments to perform time domain response history analysis. The bi-linear backbone curve of the isolator is taken into consideration while doing a nonlinear time history analysis since the bridge may experience inelastic excursion under various earthquake types (near and far fault).

The responses of the bridge are expressed in terms of pier ductility and girder displacement in the abutment, which are considered to be lognormally distributed.

Figure 4 shows the typical IDA curve and mean for displacement ductility for both near and far fault earthquakes for PGA of 0.1 g to 1.2 g. As Figure 4 shows, the response displacement ductility of the near fault earthquakes is very different from that of far fault earthquakes. The bridge begins in inelastic state at 0.42g for near fault earthquakes and 0.58g for far fault earthquakes. Also, Figure 4 shows that at PGA = 0.2g which is design level, the difference in displacement ductility requirements between near fault and far fault earthquakes are not significant. Figure 4 shows that the difference between the ductility requirements for near fault and the far fault is more noticeable when PGA = 0.6 g.

Figure 5 shows the maximum girder displacement responses and their corresponding median values for different groups of earthquakes. The peak deck displacements for the near fault are roughly three times larger than those for the far fault.

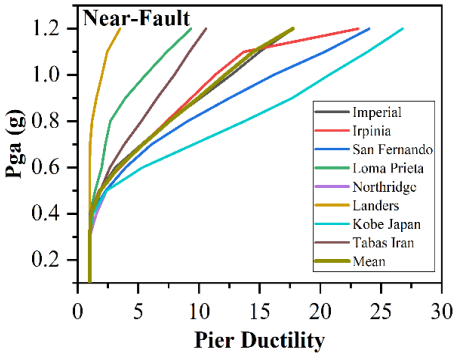

(a)

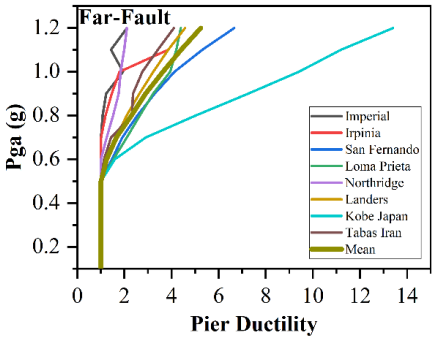

(b)

Figure 4. IDA curves for Pier Ductility: (a) Near fault; (b) Far-fault Earthquakes

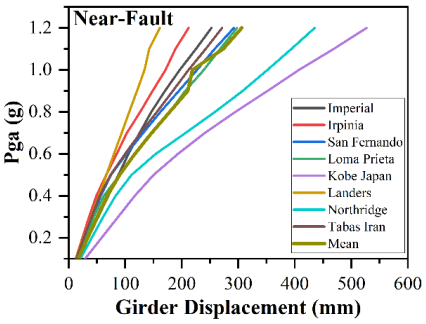

(a)

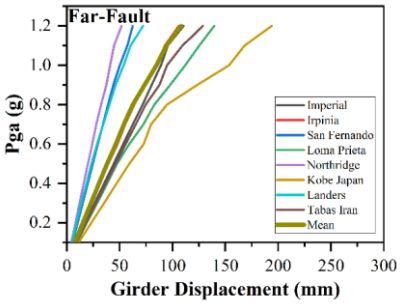

(b)

Figure 3. IDA curves for girder displacement: (a) Near fault; (b) Far-fault Earthquakes

The responses to near fault earthquakes diverge completely from those far-field earthquakes. Additionally, the pier ductility was significantly higher in

Near-fault earthquakes and exceeds the collapse damage state at 0.6 g while for the far-fault earthquakes, the bridge begins to collapse at 1g as shown in Figure .

The girder displacement responses for various earthquake types are shown in Figure 7. When compared to records from the far fault, the peak girder displacement for the close fault is approximately 2.72 times greater. When compared to the far fault effect, the amplifying response for the close fault ground motion is demonstrated to be 2.72. With a PGA of 0.8 g in the near-fault earthquake the bridge reaches a condition of collapse, as depicted in Figure 7.

A PSDM was employed in this research to construct the fragility curves from the bridge nonlinear time-history analyses. The PSDM creates a correlation between demand measures and intensity measure. The structural responses were distributed using the cloud approach, and a PSDM was created based on the results of the nonlinear time-history analysis. By employing the power-law that creates a logarithmic correlation between the median demand and chosen measure, regression analysis was utilized to obtain the mean and standard deviation for each limit condition. Figure 8 depicts a log-log plot of pier ductility and girder displacement with respect to PGA (96 data points). The structural median demands, R^2 and standard logarithmic deviation for pier and deck are listed in Table 4.

Using the described technique, fragility functions for bridges were built for the different damage measures and PGA as an intensity measure. The probability of reaching the limit states DS-1 (mild), DS-2 (modest), DS-3 (severe), and DS-4 (collapse) is depicted by the fragility curves in Figure 9.

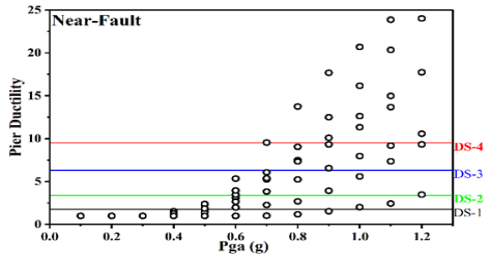

Figure 6. Response distribution for Pier Ductility: a) Near fault; b) Far-fault Earthquakes

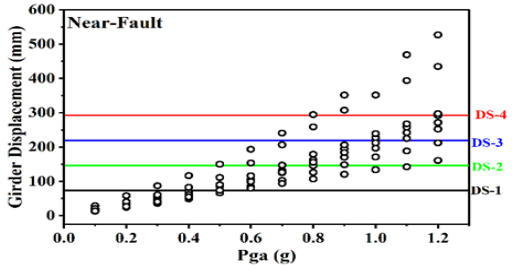

Figure 7. Response distribution for Girder Displacement: (a) Near fault; (b) Far-fault Earthquakes

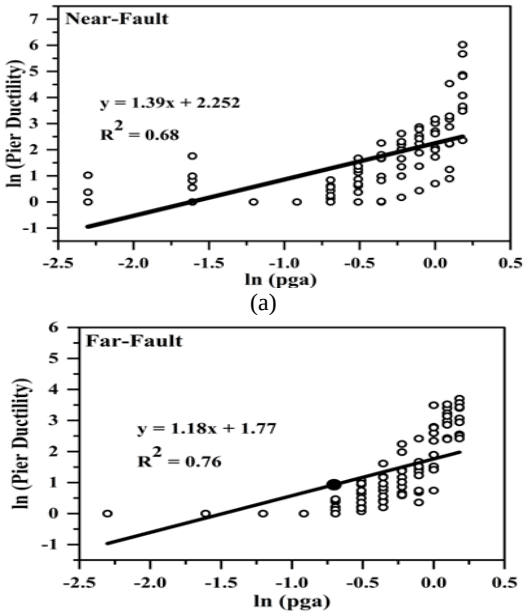

Figure 4. Logarithmic Regression Analysis for Pier Ductility: (a) Near fault; (b) Far-fault Earthquakes

TABLE 4. Proposed Damage Model for damage measures

Damage Measure	Earthquake	Damage Model	β_D	R^2
Pier Ductility	Near Fault	ln 9.50 + 1.39 ln (PGA)	1.21	0.68
Pier Ductility	Far Fault	ln 5.87 + 1.18 ln (PGA)	1.07	0.76
Girder Displacement	Near Fault	ln 340.3 + 1.38 ln (PGA)	1.12	0.85
Girder Displacement	Far Fault	ln 131.6 + 1.30 ln (PGA)	1.02	0.77

For mild (DS-1) damage scenarios related to various damage indicators, the probability of Exceedance (POE) varies substantially less between ground motions. The difference in the probability of exceedance becomes large as the damage condition advances from DS-3 to DS-4 as shown in Figure 10.

For the near-fault earthquakes, the rotational pier ductility has the POE, with 8% at 0.2g, 23% at 0.4g, and 51 % at 0.8g in severe (DS-3) damage and 5% at 0.2g, 17% at 0.4g, and 31% at 0.8g in collapse (DS-4) damage. The POE for girder displacement was 6% at 0.2g, 27% at 0.4g, and 62 % at 0.8g in severe (DS-3) damage and 3% at 0.2g, 18% at 0.4g, and 44% at 0.8g in collapse (DS-4) damage as depicted in Figure 5.

According to the current study, the POEs for far-fault earthquake for DS-3 were 1 to 5% corresponding to extreme level (PGA of 0.4g), and substantially (within 28%) at extreme-level (PGA of 0.8g), with severe and

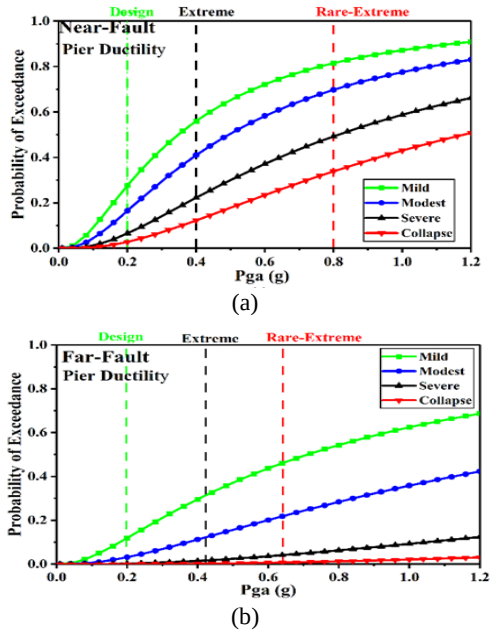

Figure 5. Fragility curve for Pier Ductility: a) Near fault; b) Far-fault Earthquakes

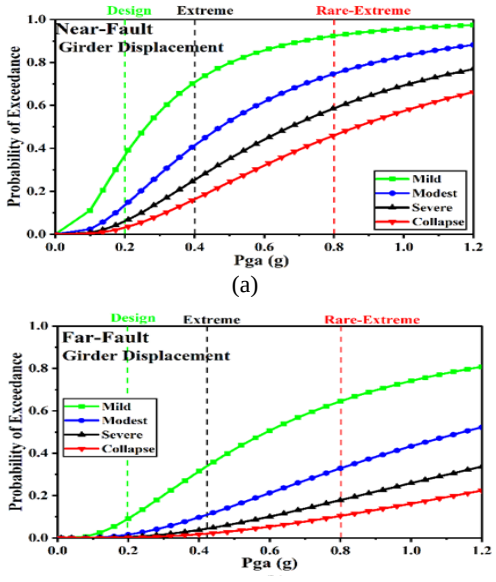

Figure 6. Fragility curve for Girder Displacement: a) Near fault; b) Far-fault Earthquakes

collapse (DS4) damage only being significant at the rare extreme-level (PGA of 0.8g) as shown in Figure 10.

8. CONCLUSIONS

To illustrate the differences in the performance of the bridge features, the performance of a tub girder bridge was examined for the near- and far-fault seismic data. The selected bridge's behavior was indicated by (i) pier ductility and (ii) girder displacement. Furthermore, the nonlinear fluctuation of the friction pendulum bearing and the plastic rotation of the bridge isolated with FPB under various forms of seismic events are explored. The analytical results of this study on a particular steel-tub girder bridge leads to the following conclusions:

- Pier ductility and girder displacement are reduced significantly in far-fault ground motions.
- Seismic isolation using friction pendulum is highly efficient in lowering ductility and girder displacement in far-field earthquakes, but it is less efficient in near-fault earthquakes.
  At a higher PGA of 0.4g, Inelastic excursions occurs on the isolated bridge.
- The highway bridge fragility curves were designed to account for four damage limit conditions. The fragility curve for the collapse damage limit condition was substantially influenced by the relative displacement of the superstructure. In contrast, the ductility requirements of the piers dominated the fragility curves for the severe and collapse damage limit states.
- Because these fragility curves were more trustworthy, it emerged that the analyses ground motion (PGA) had an accurate correlation with the seismic damage suffered by bridge components. As a result, it was found that the fragility curves produced using PGA were more accurate for evaluating the damage limit condition of the bridges.
- Even for greater PGA levels with severe and collapse damage states, the probability of exceedance for the ground motions remains significant. In the severe damage state, the POE is 24% at 0.4g and 52% at 0.8g and nearly 65% in the collapse damage state.

The information above should make it apparent that the friction pendulum bearing developed for bridges sensitive to far-fault earthquakes should not be employed in the case of near-fault earthquakes. When an earthquake occurs close to a fault, the isolator must withstand much more seismic force; for instance, the pier's ductility begins to deteriorate at a level of 0.7 g PGA. The girder displacements suffered collapse when the level of PGA was 0.8 g earthquake levels. For the peak ground acceleration of 0.6g the bridge suffers mild to moderate damage under near-fault ground motions. Therefore, the friction pendulum isolator is feasible up to 0.6g under near-fault earthquakes higher levels of PGA it is necessary to develop additional type of isolators. To allow for such large pier ductility and girder displacement without causing system instability, the pier ductility must be controlled to a lower value, necessitating a hybrid control method.

9. REFERENCES

1. Khan, B. L., Azeem, M., Usman, M., Farooq, S. H., Hanif, A., and Fawad, M. "Effect of near and far field earthquakes on performance of various base isolation systems." ***Procedia Structural Integrity***, Vol. 18, (2019), 108-118. https://doi.org/10.1016/j.prostr.2019.08.145
2. Xu, J., Li, Y., Liu, K., and Qiao, W. "Seismic Design of Tied Arch Bridge in High Earthquake Region Based on Friction Pendulum Seismic Isolation Bearing." ***IOP Conference Series: Earth and Environmental Science***, Vol. 787, No. 1, (2021). https://doi.org/10.1088/1755-1315/787/1/012172
3. Li, B., Wang, B., Wang, S., and Wu, X. "Energy response analysis of continuous beam bridges with friction pendulum bearing by multihazard source excitations" ***Shock and Vibration***, Vol. 2020, (2020). https://doi.org/10.1155/2020/3724835
4. Zhang, Y., Li, J., Wang, L., and Wu, H. "Study on the Seismic Performance of Different Combinations of Rubber Bearings for Continuous Beam Bridges." ***Advances in Civil Engineering***, Vol. 2020, (2020). https://doi.org/10.1155/2020/8810874
5. Kunde, M. C., and Jangid, R. S. "Effects of Pier and Deck Flexibility on the Seismic Response of Isolated Bridges." ***Journal of Bridge Engineering***, Vol. 11, No. 1, (2006), 109121. https://doi.org/10.1061/(asce)10840702(2006)11:1(109)
6. Li, S. Q., and Liu, H. B. "Comparison of vulnerabilities in typical bridges using macroseismic intensity scales." ***Case Studies in Construction Materials***, Vol. 16, (2022). https://doi.org/10.1016/j.cscm.2022.e01094
7. Li, S. Q., and Liu, H. B. "Analysis of probability matrix model for seismic damage vulnerability of highway bridges." ***Geomatics, Natural Hazards and Risk***, Vol. 13, No. 1, (2022), 1395–1421. https://doi.org/10.1080/19475705.2022.2077146
8. Liu, Q., and Yang, C. "Seismic damage probability assessment of isolated girder bridges based on performance under near-field earthquakes." ***Applied Sciences (Switzerland)***, Vol. 11, No. 20, (2021). https://doi.org/10.3390/app11209595
9. Afreen, A., Ahmed, A., and Moin, K. "Effect of near-field earthquake on masonry structure." ***Asian Journal of Civil Engineering***, No. 0123456789, (2021). https://doi.org/10.1007/s42107-021-00353-4
10. Bhagat, S., Wijeyewickrema, A. C., and Subedi, N. "Influence of Near-Fault Ground Motions with Fling-Step and Forward-Directivity Characteristics on Seismic Response of Base-Isolated Buildings." ***Journal of Earthquake Engineering***, Vol. 25, No. 3, (2021), 455-474. https://doi.org/10.1080/13632469.2018.1520759
11. Bhandari, M., Bharti, S. D., Shrimali, M. K., and Datta, T. K. "The Numerical Study of Base-Isolated Buildings Under Near-Field and Far-Field Earthquakes." ***Journal of Earthquake Engineering***, Vol. 22, No. 6, (2018), 989-1007. https://doi.org/10.1080/13632469.2016.1269698
12. Yadav, K. K., and Gupta, V. K. "Near-fault fling-step ground motions: Characteristics and simulation." ***Soil Dynamics and Earthquake Engineering***, Vol. 101, (2017), 90-104. https://doi.org/10.1016/j.soildyn.2017.06.022
13. Shang, J., Tan, P., Han, J., Zhang, Y., and Li, Y. "Performance of seismically isolated buildings with variable friction pendulum bearings under near-fault ground motions." ***Journal of Building Engineering***, Vol. 45, (2022), 103584. https://doi.org/10.1016/j.jobe.2021.103584
14. Sreeman, D., and Kumar Roy, B. "Optimization Study of Isolated Building using Shape Memory Alloy with Friction Pendulum System under Near-fault Excitations." ***International Journal of Engineering, Transactions A: Basics***, Vol. 35, No. 11, (2022), 2176-2185. https://doi.org/10.5829/ije.2022.35.11b.12
15. Siqi, L., Tianlai, Y., and Junfeng, J. "Empirical Seismic Vulnerability and Damage of Bottom Frame Seismic Wall Masonry Structure: A Case Study in Dujiangyan (China) Region." ***International Journal of Engineering, Transactions C: Aspects***, Vol. 32, No. 9, (2019), 1260-1268. https://doi.org/10.5829/ije.2019.32.09c.05
16. Nair, S. S., Hemalatha, G., Raja, S. R., and Stephen, E. A. "Seismic vulnerability studies of a G+17 storey building in Abu Dhabi - UAE using fragility curves." ***International Journal of Engineering, Transactions B: Applications***, Vol. 34, No. 5, (2021), 1167-1175. https://doi.org/10.5829/ije.2021.34.05b.10
17. Avşar, Ö., Yakut, A., and Caner, A. "Analytical fragility curves for ordinary highway bridges in Turkey." ***Earthquake Spectra***, Vol. 27, No. 4, (2011), 971-996. https://doi.org/10.1193/1.3651349
18. Federal Emergency Management Agency. "Hazus Earthquake Model Technical Manual ." ***Federal Emergency Management Agency***, (2020), 1-436.
19. Razmkhah, M. H., Kouhestanian, H., Shafaei, J., Pahlavan, H., and Shamekhi Amiri, M. "Probabilistic seismic assessment of moment resisting steel buildings considering soft-story and torsional irregularities." ***International Journal of Engineering, Transactions B: Applications***, Vol. 34, No. 11, (2021), 2476-2493. https://doi.org/10.5829/IJE.2021.34.11B.11
20. Shinozuka, M., Banerjee, S., and Kim, S.-H. "Statistical and Mechanistic Fragility Analysis of Concrete Bridges," (2007), 214. Retrieved from c:%5CCS%5Call refs%5Ctechnical%5CMCEER reports%5C07-0015.pdf
21. Ranjkesh, S. H., Asadi, P., and Hamadani, A. Z. "Seismic collapse assessment of deteriorating RC bridges under multiple hazards during their life-cycle." ***Bulletin of Earthquake Engineering***, Vol. 17, No. 9, (2019), 5045-5072. https://doi.org/10.1007/s10518-019-00647-8
22. Asadi, P., Nikfar, D., and Hajirasouliha, I. "Life-cycle cost based design of bridge lead-rubber isolators in seismic regions." ***Structures***, Vol. 27, (2020), 383-395. https://doi.org/10.1016/j.istruc.2020.05.056
23. Pan, Y., Agrawal, A. K., Ghosn, M., and Alampalli, S. "Seismic Fragility of Multispan Simply Supported Steel Highway Bridges in New York State. I: Bridge Modeling, Parametric Analysis, and Retrofit Design." ***Journal of Bridge Engineering***, Vol. 15, No. 5, (2010), 448-461. https://doi.org/10.1061/(asce)be.1943-5592.0000085
24. Wang, Q., Wu, Z., and Liu, S. "Seismic fragility analysis of highway bridges considering multi-dimensional performance limit state." ***Journal of Earthquake Engineering and Engineering Vibration***, Vol. 11, No. 2, (2012), 185-193. https://doi.org/10.1007/s11803-012-0109-1
25. Deepu, S. P., Prajapat, K., and Ray-Chaudhuri, S. "Seismic vulnerability of skew bridges under bi-directional ground motions." ***Engineering Structures***, Vol. 71, (2014), 150-160. https://doi.org/10.1016/j.engstruct.2014.04.013
26. Chaudhary, D., Bahadur, G., and Krishna, R. "Performance Evaluation of Seismically Isolated Bridge," Vol. 8914, (2020), 513-518.
27. Baig, M. A., Ansari, I., Islam, N., and Umair, M. "Materials Today : Proceedings Effect of lead rubber bearing on seismic performance of steel box girder bridge." ***Materials Today: Proceedings***, (2022). https://doi.org/10.1016/j.matpr.2022.04.953
28. Ghosh, G., Singh, Y., and Thakkar, S. K. "Seismic response of continuous bridge with isolation bearings." ***Proceedings of the Institution of Civil Engineers: Bridge Engineering***, Vol. 164, No. 4, (2011), 211-225. https://doi.org/10.1680/bren.2011.164.4.211
29. Phan, V., Saiidi, M. S., Anderson, J., and Ghasemi, H. "Near-

Fault Ground Motion Effects on Reinforced Concrete Bridge Columns." ***Journal of Structural Engineering***, Vol. 133, No. 7, (2007), 982-989. https://doi.org/10.1061/(asce)0733-9445(2007)133:7(982)

30. Lee, T. H., and Nguyen, D. D. "Seismic vulnerability assessment of a continuous steel box girder bridge considering influence of LRB properties." ***Sadhana - Academy Proceedings in Engineering Sciences***, Vol. 43, No. 1, (2018), 1-15. https://doi.org/10.1007/s12046-017-0774-x
31. Landi, L., Grazi, G., and Diotallevi, P. P. "Comparison of different models for friction pendulum isolators in structures subjected to horizontal and vertical ground motions." ***Soil Dynamics and Earthquake Engineering***, Vol. 81, (2016), 75-83. https://doi.org/10.1016/j.soildyn.2015.10.016

Persian Abstract

چکیده

یاتاقان آونگ اصطکاکی (FPB) به عنوان یک راه حل محبوب برای محافظت از آسیب پل ها تحت رویدادهای لرزه ای ظهور کرده است. این مطالعه تحلیل آسیب احتمالی را برای پل پیوسته تیر وان جدا شده تحت زمین لرزه های گسل نزدیک و دور با استفاده از تحلیل شکنندگی ارائه می دهد. پل پیوسته تیر وان فولادی با جداساز آونگی اصطکاکی به عنوان مکانیزم جداسازی لرزه ای در نظر گرفته می شود. به منظور نشان دادن رفتار هیسترتیک جداسازهای آونگ اصطکاکی، از یک مدل نیرو-تغییر شکل دوخطی استفاده شد. منحنی‌های شکنندگی برای اندازه‌گیری‌های آسیب مختلف از جمله شکل‌پذیری چرخشی جابجایی پایه و تیر با پیک شتاب زمین (PGA) به عنوان اندازه‌گیری شدت (IM) ایجاد شده‌اند. تحلیل‌های دینامیکی افزایشی (IDA) برای توسعه منحنی‌های شکنندگی و مدل آسیب احتمالی با در نظر گرفتن چهار حالت آسیب آستانه انجام شد. نتایج نشان می دهد که در مورد سطح PGA پایین، زلزله نزدیک به گسل منجر به احتمال زیاد بیش از حد در مورد پل تیر وان جدا شده می شود. مدل آسیب برای پایه ها و تیرها برای همبستگی سطوح پاسخ اجزا به حالت کلی خرابی پل ایجاد شد. در نهایت، توصیه هایی برای توسعه دهندگان پل در مرحله طراحی جداسازی لرزه ای پل اولیه با استفاده از جداسازهای آونگ اصطکاکی مورد بحث قرار می گیرد.